Detecting a topological transition of quantum braiding in a threefold-degenerate eigensubspace

Zhi-Wei Han,[1] Jia-Hao Liang,[1] Zhao-Xin Fu,[1] Hong-Zhi Liu,[1] Zi-Yuan Chen,[1] Meng Wang,[1] Ze-Rui He,[1] Jia-Yi Huang,[1] Qing-Xian Lv,[1,2,3,*] Kai-Yu Liao,[1,2,3,†] and Yan-Xiong Du[1,2,3,‡]

[1]*Key Laboratory of Atomic and Subatomic Structure and Quantum Control (Ministry of Education), School of Physics, South China Normal University, Guangzhou 510006, China*

[2]*Guangdong Provincial Key Laboratory of Quantum Engineering and Quantum Materials, South China Normal University, Guangzhou 510006, China*

[3]*Guangdong-Hong Kong Joint Laboratory of Quantum Matter, Frontier Research Institute for Physics, South China Normal University, Guangzhou 510006, China*

(Received 13 August 2023; accepted 2 February 2024; published 22 February 2024)

The braiding operations of quantum states have attracted substantial attention due to their great potential for realizing topological quantum computations. In this paper, we show that a threefold-degenerate eigensubspace can be obtained in a four-level Hamiltonian which is the minimal physical system. Braiding operations are proposed to apply to dressed states in the subspace. The topology of the braiding diagram can be characterized through physical methods once the sequential braiding pulses are adopted. We establish an equivalent relationship function between the permutation group and the output states where different output states correspond to different values of the function. The topological transition of the braiding happens when two operations overlap, which is detectable through the measurement of the function. Combined with the phase variation method, we can analyze the wringing pattern of the braiding. Therefore, the experimentally feasible system provides a platform to investigate braiding dynamics, the SU(3) physics, and the qutrit gates.

DOI: 10.1103/PhysRevA.109.022431

I. INTRODUCTION

Topological quantum computation has been recognized as one of the most important approaches toward realizing the fault-tolerant quantum computer [1–4]. The scheme relies on the non-Abelian anyons which exist in the degenerate eigensubspace and obey non-Abelian braiding statistics. The unitary gate operations used to realize quantum computation are carried out by braiding non-Abelian anyons and measuring the final states. The fault tolerance of the topological quantum computer arises from the nonlocal encoding of the qubits, which makes them immune to errors caused by local perturbations. There have been numerous physical systems proposed to realize topological quantum computers, i.e., the fractional-Hall states [5,6], cold atoms [7], topological superconductors [8], and the Majorana zero modes [9]. However, substantial challenges still exist in the real experimental realizations. Recently, two research groups independently realized the simulation of the Ising-type non-Abelian anyons (also called Ising anyons) in superconducting quantum simulators with serial digital quantum gates [10,11]. The non-Abelian feature and the fusion rules are experimentally simulated in such systems. The above works have demonstrated topological quantum computation to be experimentally feasible.

On the other hand, analog experiments of non-Abelian braiding operations which connect to the topological quantum gates are also investigated [12–25]. To reveal the non-Abelian characteristic, threefold-degenerate eigenstates are needed which can be constructed by single photons interacting with seven waveguide modes in photonic chips [12]. Different light-diffraction patterns correspond to different braiding orders. It is intrinsical to the geometric effects since the dynamical phases are trivial during the evolution process. Similar results are also performed in acoustic waveguide modes [14]. Furthermore, the threefold-degenerate states can be induced with two photons interacting with four waveguide modes in photonic chips, which is used to realize three-dimensional quantum holonomy [17]. At the same time, it seems that the existed braiding results have no difference from mathematical results with classical braiding (that is, braiding classical objects with different orders will obtain different final states). It would be interesting to ask whether a "quantum" braiding (braiding quantum systems with quantum controls) would be different from a "classical" braiding. To answer the above question, one may resort to a quantum system with a fully controllable Hamiltonian.

In this paper, we propose to perform non-Abelian braiding operations in a threefold-degenerate subspace in a cold atomic system. The degenerate eigensubspace is constructed in a four-level system which costs the minimal physical resources. Braiding operations of the eigenstates are introduced in such systems by imposing dressed pulses upon dressed states. Different braiding orders generate different final states

*LQX0801@163.com
†liaokaiyu1989@163.com
‡yanxiongdu@m.scnu.edu.cn

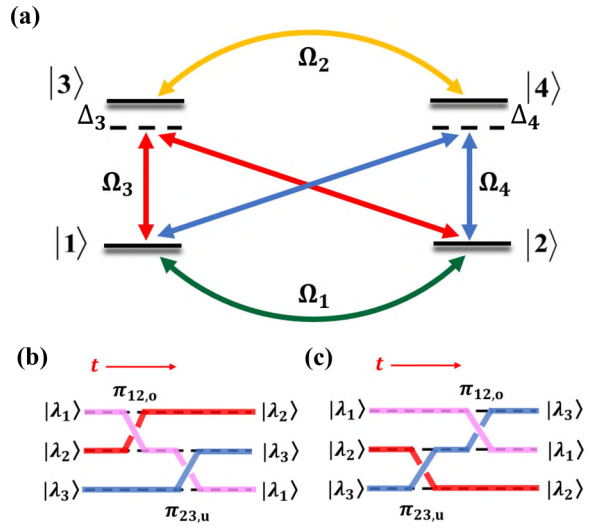

FIG. 1. (a) Coupling scheme used to achieve the threefold-degenerate eigensubspace. Bare states $\{|1\rangle, |2\rangle, |3\rangle, |4\rangle\}$ are four energy levels in a cold ^{87}Rb atomic system. Ω_1, Ω_2 are the Rabi frequencies of radio fields or two-photon Raman transitions while $\Omega_3(\Omega_4)$ with detuning $\Delta_3(\Delta_4)$ are the Rabi frequencies of microwave fields. (b) World-line description of braiding schemes of three degenerate eigenstates $\{|\lambda_1\rangle, |\lambda_2\rangle, |\lambda_3\rangle\}$. t denotes the evolving time and the solid colored lines denote the positions of the states. Different orders of braiding operations $\{\pi_{12,o}, \pi_{23,u}\}$ will induce different final states which confirms the non-Abelian characteristic of the braiding. The orientation of the braiding can be introduced by introducing the rotating direction of the π pulses where the overcrossing operation is achieved by $\pi_{kj,o}$ in Eq. (5) and the undercrossing is achieved by $\pi_{kj,u}$ in Eq. (6).

which shows the non-Abelian character. The quantumness of the braiding operations is shown by overlapping two operations that will make topological transition happen. To quantify such transitions, mapping functions that are experimentally measurable are introduced to label different final output states. Therefore, the proposal system with threefold-degenerate subspace provides an experimentally feasible way to investigate the braiding dynamics, and furthermore, the SU(3) physics [26,27]. The paper is organized as follows: In Sec. II we introduce the four-level system that generates the threefold-degenerate eigensubspace. In Sec. III we introduce the braiding operation upon dressed states and test the robustness. In Sec. IV we characterize the topology of the linking pattern by introducing an equivalence relationship which is experimentally detectable. In Sec. V we characterize the topology of the wringing pattern by testing the response to the phase variation of π pulses. We conclude the paper in Sec. VI.

II. HAMILTONIAN WITH THREEFOLD-DEGENERATE EIGENSUBSPACE

Here we construct a threefold-degenerate eigensubspace in a fully controllable cold atomic system. We adopt a four-level system interacting with six optical fields as shown in Fig. 1(a), where the energy levels are chosen to be $|1\rangle = |F = 2, m_F = -1\rangle$, $|2\rangle = |F = 1, m_F = -1\rangle$, $|3\rangle = |F = 2, m_F = 0\rangle$, and $|4\rangle = |F = 1, m_F = 0\rangle$ in the ^{87}Rb atom. Under the bare state basis $\{|1\rangle, |2\rangle, |3\rangle, |4\rangle\}$ and rotating-wave approximation, the interaction Hamiltonian is given by

$$H = \frac{1}{2}\begin{pmatrix} 0 & \Omega_1 e^{i\varphi} & \Omega_3 & \Omega_4 e^{i\varphi} \\ \Omega_1 e^{-i\varphi} & 0 & \Omega_3 e^{-i\varphi} & \Omega_4 \\ \Omega_3 & \Omega_3 e^{i\varphi} & \Delta_3 & \Omega_2 e^{i\varphi} \\ \Omega_4 e^{-i\varphi} & \Omega_4 & \Omega_2 e^{-i\varphi} & \Delta_4 \end{pmatrix}, \tag{1}$$

where we have adopted $\hbar = 1$. The Rabi frequencies $\Omega_3(\Omega_4)$ with detuning $\Delta_3(\Delta_4)$ that couple $\{|1\rangle, |3\rangle\}, \{|2\rangle, |3\rangle\}(\{|1\rangle, |4\rangle\}, \{|2\rangle, |4\rangle\})$ are set to be microwave fields, where similar experiments have been realized in [28]. The coupling $\Omega_1(\Omega_2)$ between $\{|1\rangle, |2\rangle\}(\{|3\rangle, |4\rangle\})$ can be realized by radio fields [29,30] or two-photon Raman transitions [31]. One can find that when the detuning satisfies conditions $\Delta_3 = \Omega_3^2/\Omega_1 - \Omega_1$, $\Delta_4 = \Omega_4^2/\Omega_1 - \Omega_1$, $\Omega_1\Omega_2 = \Omega_3\Omega_4$, the eigenvalues of Hamiltonian (1) are given by

$$\lambda_1 = \lambda_2 = \lambda_3 = -\Omega_1, \quad \lambda_4 = \frac{\Omega_1^2 + \Omega_2^2 + \Omega_3^2}{\Omega_1^2}, \tag{2}$$

of which a threefold-degenerate subspace with the lowest eigenvalues exists. Comparing with the seven-level scheme [12] or the N-pod system [32,33], the proposed system is the minimal physical one, promoting experimental feasibility. By parametrizing $\Omega_1 = \Omega_0 \sin\alpha \sin\theta$, $\Omega_2 = 2\Omega_0 \cos\alpha/\tan\theta$, $\Omega_3 = \sqrt{2}\Omega_0 \sin\alpha \cos\theta$, $\Omega_4 = \sqrt{2}\Omega_0 \cos\alpha$, the eigenstates will be obtained as

$$\begin{aligned} |\lambda_1\rangle &= \frac{\sqrt{2}}{2}(|1\rangle - e^{-i\varphi}|2\rangle), \\ |\lambda_2\rangle &= \cos\theta|b\rangle - \sin\theta|3\rangle, \\ |\lambda_3\rangle &= \cos\alpha|c\rangle - e^{-i\varphi}\sin\alpha|4\rangle, \\ |\lambda_4\rangle &= \sin\alpha|c\rangle + e^{-i\varphi}\cos\alpha|4\rangle, \end{aligned} \tag{3}$$

where $|b\rangle = \sqrt{2}/2(|1\rangle + e^{-i\varphi}|2\rangle)$, $|c\rangle = \sin\theta|b\rangle + \cos\theta|3\rangle$. Under the subspace spanned by the lowest eigenstates, one will obtain the non-Abelian gauge potentials and gauge fields as calculated by $A_\mu^{jk} = i\langle\lambda_j|\partial_\mu|\lambda_k\rangle$ (A_μ^{jk} are the matrix elements of $A_{lm,\mu}$ defined in two of the threefold eigenstates, i.e., the subspace of $\{|\lambda_1\rangle, |\lambda_2\rangle\}$) and $F_{lm,\mu\nu} = \partial_\mu A_{lm,\nu} - \partial_\nu A_{lm,\mu} - i[A_{lm,\mu}, A_{lm,\nu}]$, respectively [34,35]. Using Eq. (3), the nondiagonal matrix of SU(3) gauge field $F_{lm,\theta\alpha}$ will be given by

$$\begin{aligned} F_{12,\theta\alpha} &= F_{13,\theta\alpha} = 0, \\ F_{23,\theta\alpha} &= i\begin{pmatrix} 0 & \dot{\theta}\dot{\alpha}\sin\alpha \\ -\dot{\theta}\dot{\alpha}\sin\alpha & 0 \end{pmatrix}. \end{aligned} \tag{4}$$

Therefore, the threefold-degenerate eigensubspace provides a fully controllable platform to investigate the braiding dynamics and the evolution will be determined by geometric characteristics of the gauge field which can be treated as geometric quantum control [36–46].

III. BRAIDING OPERATION OF DRESSED STATES AND ROBUSTNESS

In the following, we discuss the braiding operations in the eigensubspace constructed by $\{|\lambda_1\rangle, |\lambda_2\rangle, |\lambda_3\rangle\}$. Considering the oriented link of the braiding configuration [47–49], the overcrossing braiding operation can be realized by π pulses upon dressed states defined as

$$\pi_{kj,\mathrm{o}} = -i(|\lambda_k\rangle\langle\lambda_j|e^{i\phi_{kj}} + |\lambda_j\rangle\langle\lambda_k|e^{-i\phi_{kj}}) + |\lambda_l\rangle\langle\lambda_l| + |\lambda_4\rangle\langle\lambda_4|, \tag{5}$$

where $k, j, l = 1, 2, 3$. And the undercrossing braiding is defined as

$$\pi_{kj,\mathrm{u}} = i(|\lambda_k\rangle\langle\lambda_j|e^{i\phi_{kj}} + |\lambda_j\rangle\langle\lambda_k|e^{-i\phi_{kj}}) + |\lambda_l\rangle\langle\lambda_l| + |\lambda_4\rangle\langle\lambda_4|, \tag{6}$$

which satisfies the relationships $\pi_{kj,\mathrm{o}}\pi_{kj,\mathrm{o}} = \pi_{kj,\mathrm{u}}\pi_{kj,\mathrm{u}} = -1$, $\pi_{kj,\mathrm{o}}\pi_{kj,\mathrm{u}} = \pi_{kj,\mathrm{u}}\pi_{kj,\mathrm{o}} = 1$ [50]. It can be seen that the orientation of the crossing is equivalent to the rotating direction of the quantum states along a certain axis. Once the mapping between the braiding and the π pulses sequences is established, we can investigate the topology of the braiding in the dressed states subspace.

The π pulse $\pi_{kj,\mathrm{o}}$ is connected to the evolution governed by the Hamiltonian H_{kj} with $\pi_{kj,\mathrm{o}} = e^{-iH_{kj}T}$ and $\pi_{kj,\mathrm{u}} = e^{iH_{kj}T}$, where T is the evolution period. To simplify the experimental realization, we set the initial control parameters with $\theta(t=0) = \pi/2, \alpha(t=0) = \pi/2, \varphi(t=0) = 0$ [51] where the eigenstates turn out to be

$$|\lambda_1\rangle_{\mathrm{in}} = \tfrac{\sqrt{2}}{2}(|1\rangle - |2\rangle), \quad |\lambda_2\rangle_{\mathrm{in}} = -|3\rangle,$$
$$|\lambda_3\rangle_{\mathrm{in}} = -|4\rangle, \quad |\lambda_4\rangle_{\mathrm{in}} = \tfrac{\sqrt{2}}{2}(|1\rangle + |2\rangle). \tag{7}$$

In this case, we find that the braiding operations $\pi_{12,0}, \pi_{23,\mathrm{u}}$ with $\phi_{12} = \phi_{23} = \phi$ can be realized by the Hamiltonian under the bare states basis $\{|1\rangle, |2\rangle, |3\rangle, |4\rangle\}$ with

$$H_{12} = \frac{\Omega_{12}}{4}\begin{pmatrix} 0 & 0 & -\sqrt{2}e^{i\phi} & 0 \\ 0 & 0 & \sqrt{2}e^{i\phi} & 0 \\ -\sqrt{2}e^{-i\phi} & \sqrt{2}e^{-i\phi} & 0 & 0 \\ 0 & 0 & 0 & 0 \end{pmatrix}, \tag{8}$$

$$H_{23} = \frac{\Omega_{23}}{2}\begin{pmatrix} 0 & 0 & 0 & 0 \\ 0 & 0 & 0 & 0 \\ 0 & 0 & 0 & e^{i\phi} \\ 0 & 0 & e^{-i\phi} & 0 \end{pmatrix}, \tag{9}$$

with $\Omega_{12}T = \Omega_{23}T = \pi$. It can be seen that H_{12} can be realized by a triangle-type three-level system [45] while H_{23} is achieved by coupling the two-level system $\{|3\rangle, |4\rangle\}$.

As shown in Figs. 1(b) and 1(c), braiding operations of groups $\{\pi_{12,\mathrm{o}}, \pi_{23,\mathrm{u}}\}$ are introduced, where $\pi_{12,\mathrm{o}}$ is used to inverse the population of dressed states $|\lambda_1\rangle$ and $|\lambda_2\rangle$, and $\pi_{23,\mathrm{u}}$ is used to inverse the population of dressed states $|\lambda_2\rangle$ and $|\lambda_3\rangle$. Mathematically, the final braiding states are determined by the orders of braiding operations which reveal the non-Abelian characteristic. For example, when the systems are prepared in the state $|\Psi_0\rangle = a_1|\lambda_1\rangle + a_2|\lambda_2\rangle + a_3|\lambda_3\rangle + a_4|\lambda_4\rangle$, the final state will be $|\Psi_1\rangle = a_2|\lambda_1\rangle + a_3|\lambda_2\rangle + a_1|\lambda_3\rangle + a_4|\lambda_4\rangle$ against the union operations $\pi_{23,\mathrm{u}}\pi_{12,\mathrm{o}}$ [Fig. 1(b)], while $|\Psi_2\rangle = a_3|\lambda_1\rangle + a_1|\lambda_2\rangle + a_2|\lambda_3\rangle + a_4|\lambda_4\rangle$ corresponds to the one of $\pi_{12,\mathrm{o}}\pi_{23,\mathrm{u}}$ [Fig. 1(c)]. To detect the final output state, one needs to measure the population on each eigenstates which is done by applying a $\pi/2$ pulse to $\{|1\rangle, |2\rangle\}$. Therefore, the correspondence between the final braiding states and the bare states will be given by $|\lambda_1\rangle_f = |1\rangle$, $|\lambda_2\rangle_f = -|3\rangle$, $|\lambda_3\rangle_f = -|4\rangle$, $|\lambda_4\rangle_f = |2\rangle$ and the eigenstates can be detected by measuring the bare states.

In Figs. 2(a) and 2(b), the population dynamics of the braiding upon dressed states representations are depicted. The initial state is chosen to be $|\Psi_0\rangle = \sqrt{0.4}|\lambda_1\rangle + \sqrt{0.3}|\lambda_2\rangle + \sqrt{0.2}|\lambda_3\rangle + \sqrt{0.1}|\lambda_4\rangle$, and Fig. 2(a) shows the results of operations $\pi_{23,\mathrm{u}}\pi_{12,\mathrm{o}}$ while Fig. 2(b) shows the ones of operations $\pi_{12,\mathrm{o}}\pi_{23,\mathrm{u}}$, with $\phi = \pi/2$. To investigate the general dynamics, Hamiltonian (1) with $\theta = \pi/2$, $\alpha = \pi/2$, and $\varphi = 0$ is applied between the gap of the braiding pulses which makes the system always evolve in the eigensubspace [52]; that is, the evolution is given by

$$U = U_H(T_3)U_\pi(T)U_H(T_2)U_\pi(T)U_H(T_1); \tag{10}$$

$U_H(T_i) = e^{-iHT_i}; i = 1, 2, 3$; T_i is the interaction duration of H; $U_\pi(T) = \{\pi_{23,\mathrm{u}}, \pi_{12,\mathrm{o}}\}$. In the numerical simulation, we set $\Omega_{12} = \Omega_{23} = 1$ and $T_1 = T_2 = T_3 = T = \pi$. U_H will not change the population upon the eigenstates since $|\lambda_i\rangle_{\mathrm{in}}, i = 1, 2, 3$ are the instantaneous eigenstates of H. As shown in Figs. 2(a) and 2(b), the different braiding results of different braiding orders truly reveal the non-Abelian characteristic.

Here we discuss the robustness of braiding, as shown in Fig. 2(c). Assuming the starting time of $\pi_{12,\mathrm{o}}(\pi_{23,\mathrm{u}})$ is set to be $t_1(t_2)$, we tilt $t_1(t_2)$ and observe the final population of union operations $\pi_{23,\mathrm{u}}\pi_{12,\mathrm{o}}$. It can be seen that $t_1 = T_1, t_2 = T_1 + T + T_2$. By keeping the separation $\Delta t = t_2 - t_1 > T$ (two braiding operations do not overlap), the population P_1 of eigenstate $|\lambda_1\rangle$ does not change along with t_1 and Δt (other populations are also similar with P_1). Such robustness is guaranteed by the topology of the braiding which does not change as long as one changes the control parameters.

IV. CHARACTERIZING THE LINKING PATTERN AND TOPOLOGICAL TRANSITION

In the following, we discuss how to characterize the braiding configuration with physical methods in the dressed state subspace, and make a comparison with the one in mathematic theory.

We first briefly review how to characterize the topology of braiding in mathematic theory [47–49,53]. Since the braiding diagrams can be changed to knots by certain rules, we use the language of knot theory in the following. To determine the topology, one needs to quantify the linking patterns (the numbers and the distribution of the crossing) and wringing patterns (the orientation of the crossing) which utilize the Jones polynomial. Given an oriented link L, the Jones polynomial is given by $X(L) = (-A^3)^{-\omega(L)}\langle L\rangle$, where A is a variable, $\langle L\rangle$ is the bracket polynomial that characterizes the linking patterns of L, and $\omega(L)$ is the writhe that characterizes the wringing patterns of L. It can be found that the topological invariant in knot theory is different from the Chern number in condensed-matter physics which is defined as an integral of

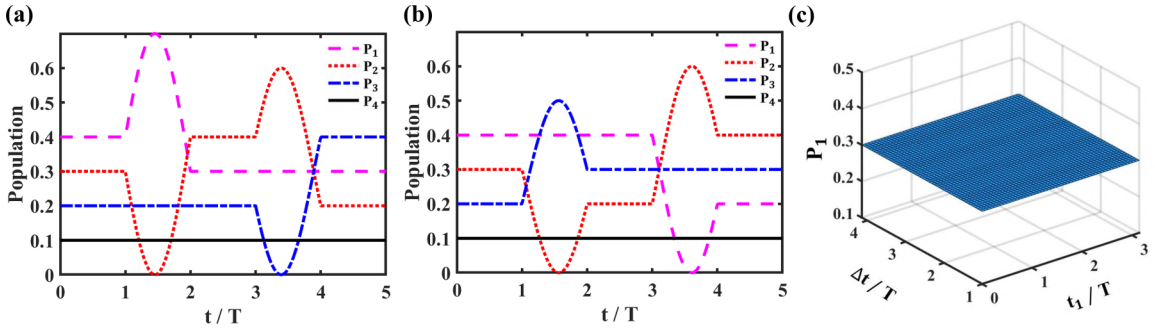

FIG. 2. The braiding dynamics and their robustness. (a) The braiding dynamics of union operation $\pi_{23,u}\pi_{12,o}$. (b) The braiding dynamics of union operation $\pi_{12,o}\pi_{23,u}$. The initial states of both cases are set to be $|\Psi_0\rangle = \sqrt{0.4}|\lambda_1\rangle + \sqrt{0.3}|\lambda_2\rangle + \sqrt{0.2}|\lambda_3\rangle + \sqrt{0.1}|\lambda_4\rangle$. Hamiltonian (1) with $\theta = \pi/2$, $\alpha = \pi/2$, and $\varphi = 0$ is introduced between the gap of the braiding pulses which makes the system always evolve in the eigensubspace. The evolution is thus governed by $U = U_H(T_3)U_\pi(T)U_H(T_2)U_\pi(T)U_H(T_1)$, $U_\pi(T) = \{\pi_{12,o}, \pi_{23,u}\}$, $T_1 = T_2 = T_3 = T$, where T is the evolution period of the braiding pulses. Pink dashed lines, population of $|\lambda_1\rangle$, P_1; red dotted lines, population of $|\lambda_2\rangle$, P_2; blue dash-dotted lines, population of $|\lambda_3\rangle$, P_3; black solid lines, population of $|\lambda_4\rangle$, P_4; the population of eigenstates can be detected by the ones of bare states with suitable pulses. (c) Population P_1 vs starting time t_1 and the time interval Δt.

the gauge field (described by the mathematics called differential geometry) [28,29,54–56].

In the following, we will introduce how to characterize the topology of braiding in dressed state subspace with physical methods.

We first discuss the characterization of the linking pattern of the braiding. Assuming that there are m input states with the population denoted as P_i, $i = 1, 2, \ldots, m$ with $P_1 > P_2 > \cdots > P_m$. We can redefine P_i by $P_i' = m + 1 - i$. One can find that the final output state after braiding will be one of the permutations of arrangement $(P_1'P_2' \ldots P_m')$ which can be marked as

$$\xi = \begin{pmatrix} P_1' & P_2' & \cdots & P_m' \\ A_1 & A_2 & \cdots & A_m \end{pmatrix}. \tag{11}$$

Then we map the permutation ξ to a one to one function as

$$K(\xi) = \prod_i (A_i)^i. \tag{12}$$

K is experimentally determined from the population P_i. It is known that the permutation groups are the invariant subgroup of braiding groups [48] and the output result will not be changed by the three Reidemeister moves in knot theory; function K can be treated as an equivalence relationship which separates the braiding into several groups. Since the braiding scheme with N crossing will have 2^N possible kinds of configuration and m states will have $m!$ possible permutations, we can construct a physical system with big enough m to cover the possible configurations of the braiding.

In Fig. 3(a), index K versus separation time Δt of two braiding operations $\{\pi_{23,u}, \pi_{12,o}\}$ are depicted for the case of $m = 3$. The initial state is chosen to be $|\Psi_0\rangle$ (the same as in Fig. 2). The fully controllable quantum system offers a platform to investigate the topological transition dynamics of braiding. When $\Delta t > \pi$, two braiding operations are well separated; K is stable at 54 as the given final state $|\Psi_1\rangle = \sqrt{0.3}|\lambda_1\rangle + \sqrt{0.2}|\lambda_2\rangle + \sqrt{0.4}|\lambda_3\rangle + \sqrt{0.1}|\lambda_4\rangle$ after the union operations $\pi_{23,u}\pi_{12,o}$. K will be stable at 72 when $\Delta t < -\pi$, where final state $|\Psi_2\rangle = \sqrt{0.2}|\lambda_1\rangle + \sqrt{0.4}|\lambda_2\rangle + \sqrt{0.3}|\lambda_3\rangle + \sqrt{0.1}|\lambda_4\rangle$ after the union operation $\pi_{12,o}\pi_{23,u}$. As can be seen that the output states are robust against the separation time between pulses if the pulses are well separated. The above classification results are in accord with the ones of the bracket polynomial $\langle L\rangle$. To calculate $\langle L\rangle$, we insert the braiding $\{\pi_{23,u}, \pi_{12,o}\}$ in a nontrivial knot which induces $\langle L\rangle = 1$ for the case $\pi_{23,u}\pi_{12,o}$ and $\langle L\rangle = -2$ for the case $\pi_{12,o}\pi_{23,u}$.

When $-\pi < \Delta t < \pi$, braiding operations overlap. Here K is sensitive to Δt since the overlapping states are not topological. Therefore, we can detect the dynamics of topological transition in the dressed states subspace which cannot be realized in classical systems.

V. CHARACTERIZING THE WRINGING PATTERN WITH PHASE VARIATION

Here we discuss the characterization of the wringing pattern of the braiding. As for the oriented link, the linking pattern is not enough to determine the topology of the braiding. Different from the writhe $\omega(L)$ in the Jones polynomial, here we propose to investigate the wringing patterns with the phase dynamics of the quantum systems. To test the phase coherence of the operations $\pi_{23,u}\pi_{12,o}$, we tilt the relative

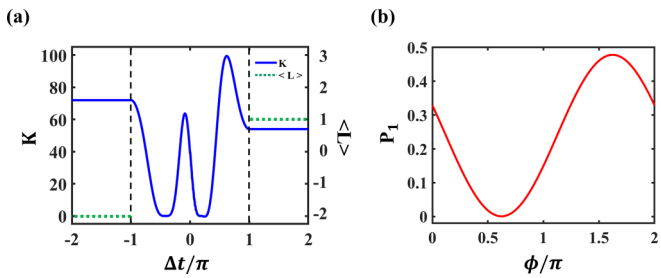

FIG. 3. (a) Equivalent relationship function K of braiding $\{\pi_{23,u}, \pi_{12,o}\}$ vs the deviation of Δt. $\Delta t > \pi$ and $\Delta t < -\pi$ correspond to two different braiding configurations and K will change accordingly. The classification of topology by K is the same as the bracket polynomial $\langle L\rangle$ in the well-defined regions. The topological transition will happen when two braiding pulses overlap of which the dynamics can be described by K. (b) Relationship between population P_1 and the relative phase ϕ. The phase coherence shows the quantumness of the braiding.

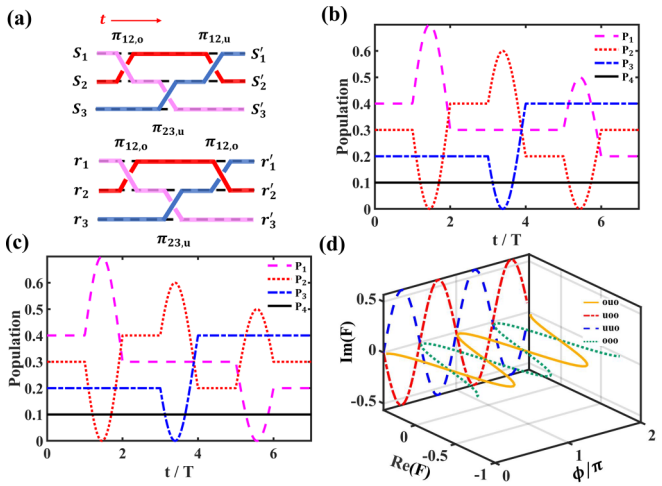

FIG. 4. (a) World-line description of braiding $\pi_{12,u}\pi_{23,u}\pi_{12,o}$ (upper panel) and $\pi_{12,o}\pi_{23,u}\pi_{12,o}$ (bottom panel) where only the orientations of the final π pulses of the two braiding are different. (b) Population dynamics against braiding $\pi_{12,u}\pi_{23,u}\pi_{12,o}$. (c) Population dynamics against braiding $\pi_{12,o}\pi_{23,u}\pi_{12,o}$. Pink dashed lines, population of $|\lambda_1\rangle$, P_1; red dotted lines, population of $|\lambda_2\rangle$, P_2; blue dash-dotted lines, population of $|\lambda_3\rangle$, P_3; black solid lines, population of $|\lambda_4\rangle$, P_4. (d) Inner product $F = \langle\Psi_f|\Psi_i\rangle$ vs the phase variation of the π pulses: $|\Psi_i\rangle$, the initial state; $|\Psi_f\rangle$, the final state; Re(F), the real part of F; Im(F), the imaginary part of F. Yellow solid line, braiding of $\pi_{12,o}\pi_{23,u}\pi_{12,o}$; red dash-dotted line, braiding of $\pi_{12,u}\pi_{23,o}\pi_{12,o}$; blue dashed line, braiding of $\pi_{12,u}\pi_{23,u}\pi_{12,o}$; green dotted line, braiding of $\pi_{12,o}\pi_{23,o}\pi_{12,o}$. All the calculations use the same initial state $|\Psi_0\rangle$ as in Fig. 2.

phases between the two braiding operations and calculate the final states, as described in Fig. 3(b). We set $\phi_{12} = 0$ and change ϕ from 0 to 2π in H_{23}. The final population of P_1 will change along with ϕ. Similar cases happen in P_2 and P_3 which will not happen in classical braiding. Therefore, the dynamics of braiding in quantum systems will be more interesting and may lead to novel phenomena.

In Fig. 4, we discuss the braiding with three braiding pulses by two cases: $\pi_{12,u}\pi_{23,u}\pi_{12,o}$ [upper panel in Fig. 4(a)] and $\pi_{12,o}\pi_{23,u}\pi_{12,o}$ [bottom panel in Fig. 4(a)], where the only difference between the two braiding is the orientation of the final pulses. Such braiding schemes are frequently studied in the investigation of Yang-Baxter equations [57–59]. The population dynamics in Fig. 4(b) corresponds to the braiding $\pi_{12,u}\pi_{23,u}\pi_{12,o}$ and the one in Fig. 4(c) corresponds to the braiding $\pi_{12,o}\pi_{23,u}\pi_{12,o}$, where the input state $|\Psi_0\rangle$ is the same as Fig. 2. Since the populations of the output states for both of the braiding are the same, function K cannot distinguish the two braidings. The problem also exists in the bracket polynomial $\langle L\rangle$ in knot theory. By connecting the starting point and the ending point that lay in the same dashed lines in the world-lines description of the braiding [i.e., s_1 and s_1', s_2 and s_2', and s_3 and s_3' in Fig. 4(a)], we will obtain knots or chains from the braiding diagram in Fig. 4(a), where both braiding diagrams give the same value of $\langle L\rangle = -2$. To further characterize the topology, we calculate the final states $|\Psi_f\rangle$ against the variation of the phase ϕ_{kj} in the π pulses of Eqs. (5) and (6). In Fig. 4(d), we plot the results of $F = \langle\Psi_f|\Psi_i\rangle$ against ϕ of which the y axis symbolizes the values of the real parts Re(F) and the z axis symbolizes the values of the imaginary parts Im(F) of F. As can be seen, the response curve of braiding $\pi_{12,u}\pi_{23,u}\pi_{12,o}$ [blue-dashed line in Fig. 4(d)] is different from the one of $\pi_{12,o}\pi_{23,u}\pi_{12,o}$ [yellow-solid line in Fig. 4(d)]. Other cases of braiding $\pi_{12,u}\pi_{23,o}\pi_{12,o}$ (red dash-dotted line) and $\pi_{12,o}\pi_{23,o}\pi_{12,o}$ (green dotted line) are also plotted where the response curves against the phase variation are all different. The above classification results are similar to the ones of using writhe ω in the Jones polynomial. By defining the overcrossing to be the positive crossing and the undercrossing to be the negative crossing, the writhe (number of positive crossings minus the number of negative crossings) will also derive four possible values ± 3 and ± 1 [60]. Therefore, the phase coherence of the quantum system offers a physical method to investigate the topology of the braiding.

VI. SCALABILITY OF THE PROPOSED SYSTEM

Here we discuss the scalability of the proposed system. According to the above discussion, one can achieve a $(N-1)$-fold degenerate eigensubspace from a N-level system. Considering the present experimental system, the maximal controllable levels will be $N_{\max} = 128$ with the hyperfine ground states in the holmium atom [61,62]. To achieve a larger Hilbert space, one may adopt the multiparticle states of the interacting system instead of the atomic levels, i.e., N interacting two-level atoms correspond to 2^N possible states. Assuming that an input state is given by $|\Psi_0\rangle = \sum_i c_i|\xi_i\rangle$, where $|\xi_i\rangle$ is one of the possible multiparticle states $|\xi_i\rangle = |\varepsilon_1\rangle \otimes |\varepsilon_2\rangle \cdots \otimes |\varepsilon_N\rangle$, $|\varepsilon_k\rangle, k = 1, \ldots, N$, are the quantum states of the kth two-level atom which is labeled by $\{|0\rangle, |1\rangle\}$. The braiding operation between $|\xi_k\rangle$ and $|\xi_j\rangle$ is given by

$$\pi'_{kj,\mathrm{o(u)}} = \mp i(|\xi_k\rangle\langle\xi_j|e^{i\phi_{kj}} + |\xi_j\rangle\langle\xi_k|e^{-i\phi_{kj}}) + \sum_{l\neq k,j} |\xi_l\rangle\langle\xi_l|, \tag{13}$$

which can be realized by the evolution $\pi'_{kj,\mathrm{o(u)}} = e^{\mp i\int_0^{T_I} H'_{kj}t}$ governed by the Hamiltonian $H'_{kj} = \frac{\Omega_{kj}}{2}(|\xi_k\rangle\langle\xi_j|e^{i\phi_{kj}} + |\xi_j\rangle\langle\xi_k|e^{-i\phi_{kj}})$, with $\Omega_{kj}T_I = \pi$. Hamiltonian H'_{kj} can be constructed in a N-particles system physically with Ising-type interaction as given by

$$H_I = \sum_i \left(a_i\sigma_x^i + b_i\sigma_y^i + c_i\sigma_z^i\right) + \sum_{i<j} V_{ij}\sigma_{ij}, \tag{14}$$

where $\sigma_l^i = I \otimes I \cdots \otimes \sigma_l \otimes \cdots I$, $\sigma_l (l = x, y, z)$ are the Pauli matrices applied to the ith particle, and the coefficients a_i, b_i, c_i can be time or site dependent. V_{ij} are the nearest-neighbor coupling strength and σ_{ij} are the coupling terms which have the form $\sigma_l^i\sigma_l^j$ or $\sigma_+^i\sigma_-^j + \sigma_-^i\sigma_+^j$, $\sigma_+^{i(j)} = (\sigma_x^{i(j)} + i\sigma_y^{i(j)})/2$, and $\sigma_-^{i(j)} = (\sigma_x^{i(j)} - i\sigma_y^{i(j)})/2$ [63–65]. By choosing suitable coefficients a_i, b_i, c_i, V_{ij}, Hamiltonian H'_{kj} can be realized by H_I, i.e., given an initial state $|\Psi_0\rangle = k_{00}|00\rangle + k_{11}|11\rangle)$, $(k_{00}^2 + k_{11}^2 = 1)$, the braiding operation of $\{|00\rangle, |11\rangle\}$ can be realized by $H_I = \Omega_I(\sigma_x^1\sigma_x^2 + \sigma_y^1\sigma_y^2)/4$, $\Omega_I T_I = \pi$. To discuss the dynamics in the degenerate eigensubspace, one may adopt a suitable coupling configuration

such as Hamiltonian (1) in the basis of $\{|\xi_i\rangle\}$. Therefore, the system can be extended to the Hilbert space with dimension 2^N in a N-particles system.

VII. CONCLUSION

In summary, we have proposed a scheme to realize braiding operations in a threefold-degenerate eigensubspace of a four-level system which is also the minimal physical system. The topological transition and phase coherence of the braiding factually exhibit the distinction between the quantum system and the classical system. Furthermore, we show that an equivalent relationship function and phase-variation method can be combined to classify the topology of the braiding. As known, classifications of knots are an NP problem in knot theory which is still challenging [49]. Our paper may provide a feasible way to solve the problem with physical resources.

ACKNOWLEDGMENTS

This work was supported by the National Natural Science Foundation of China (Grants No. 12074132, No. 12304287, and No. 12247123), China Postdoctoral Science Foundation (Grants No. 2022M721222 and No. 2023T160233), Natural Science Foundation of Guangdong Province (Grant No. GDZX2303006), and Guangdong Basic and Applied Basic Research Foundation (Grants No. 2021A1515110668 and No. 2023A1515011550).

Z.-W.H. and J.-H.L. contributed equally to this work.

APPENDIX: REMARKS

1. Derivation of the four-level system with a threefold-degenerate eigensubspace

To construct a four-level system with a threefold-degenerate eigensubspace directly is quite a challenging task. At the same time, it is well known that a N-pod system has a degenerate eigensubspace with $N-2$ dimensions. Therefore, we may get the four-level system with a threefold-degenerate eigensubspace deduced from the five-pod system with large detuning. Under the bare state basis $\{|1\rangle, |2\rangle, |3\rangle, |4\rangle, |5\rangle\}$ and rotating-wave approximation, the interacting Hamiltonian of a five-pod system is given by

$$H(t)=\frac{\hbar}{2}\begin{pmatrix} 0 & 0 & 0 & 0 & \Omega_1' \\ 0 & 0 & 0 & 0 & \Omega_2' e^{-i\varphi} \\ 0 & 0 & 0 & 0 & \Omega_3' \\ 0 & 0 & 0 & 0 & \Omega_4' e^{-i\varphi} \\ \Omega_1' & \Omega_2' e^{i\varphi} & \Omega_3' & \Omega_4' e^{i\varphi} & -2\Delta_5 \end{pmatrix}, \quad \text{(A1)}$$

where $\Omega_i'(i=1,2,3,4,5)$ are the Rabi frequencies and Δ_5 is the single-photon detuning. According to the Schrödinger equation and the large detuning situation ($\Delta_5 \gg \Omega_i'$), we can get

$$\begin{aligned}
\frac{dc_1}{dt} &= -\frac{i\Omega_1'}{4\Delta_5}(\Omega_1' c_1 + \Omega_2' e^{i\varphi} c_2 + \Omega_3' c_3 + \Omega_4' e^{i\varphi} c_4), \\
\frac{dc_2}{dt} &= -\frac{i\Omega_2'}{4\Delta_5}(\Omega_1' e^{-i\varphi} c_1 + \Omega_2' c_2 + \Omega_3' e^{-i\varphi} c_3 + \Omega_4' c_4), \\
\frac{dc_3}{dt} &= -\frac{i\Omega_3'}{4\Delta_5}(\Omega_1' c_1 + \Omega_2' e^{i\varphi} c_2 + \Omega_3' c_3 + \Omega_4' e^{i\varphi} c_4), \\
\frac{dc_4}{dt} &= -\frac{i\Omega_4'}{4\Delta_5}(\Omega_1' e^{-i\varphi} c_1 + \Omega_2' c_2 + \Omega_3' e^{-i\varphi} c_3 + \Omega_4' c_4),
\end{aligned} \quad \text{(A2)}$$

where c_i are the probability amplitude of bare states $|i\rangle$, $i=1,2,3,4$, respectively. One can find that the effective four-level system upon bare states $\{|1\rangle, |2\rangle, |3\rangle, |4\rangle\}$ is given by

$$H_{\text{eff}}=\frac{\hbar}{2}\begin{pmatrix} 0 & \Omega_{11} e^{i\varphi} & \Omega_{13} & \Omega_{14} e^{i\varphi} \\ \Omega_{11} e^{-i\varphi} & 0 & \Omega_{13} e^{-i\varphi} & \Omega_{14} \\ \Omega_{13} & \Omega_{13} e^{i\varphi} & \Delta_{31} & \Omega_{34} e^{i\varphi} \\ \Omega_{14} e^{-i\varphi} & \Omega_{14} & \Omega_{34} e^{-i\varphi} & \Delta_{41} \end{pmatrix}, \quad \text{(A3)}$$

with $\Omega_{11}=\Omega_1'^2/2\Delta_5$, $\Omega_{13}=\Omega_1'\Omega_3'/2\Delta_5$, $\Omega_{14}=\Omega_1'\Omega_4'/2\Delta_5$, $\Omega_{34}=\Omega_3'\Omega_4'/2\Delta_5$, $\Delta_{31}=(\Omega_3'^2-\Omega_1'^2)/2\Delta_5$, $\Delta_{41}=(\Omega_4'^2-\Omega_1'^2)/2\Delta_5$, and $\Omega_1'=\Omega_2'$. One can check that Hamiltonian H_{eff} has a threefold-degenerate eigensubspace. By replacing Ω_{11} with Ω_1, Ω_{13} with Ω_3, Ω_{14} with Ω_4, Ω_{34} with Ω_2, Δ_{31} with Δ_3, and Δ_{41} with Δ_4, we can recover Hamiltonian (1) from Hamiltonian (A3).

By adopting $(N+1)$-pod configuration, the N-fold degenerate subspace can be deduced after the reduction. It can be found that a fully connected coupling should be realized in the reduced Hamiltonian which may be experimentally challenging for large N. To solve this problem, the series-connected tripod system can be adopted [12]. It can be checked that a Hamiltonian with terms coupling the nearest neighbor is needed after the reduction, which will improve the experimental feasibility.

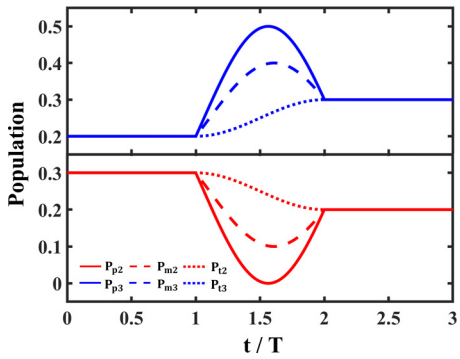

FIG. 5. Population dynamics of different input states where the density matrix is described by Eq. (A4). The coherence of input states can be tilted by parameter η. Solid lines (P_{p2}, P_{p3}), $\eta=1$; dashed lines (P_{m2}, P_{m3}), $\eta=1/2$; dotted line (P_{t2}, P_{t3}), $\eta=0$. The red lines are the numerical results of dressed state $|\lambda_2\rangle$ and the blue lines are the ones of $|\lambda_3\rangle$.

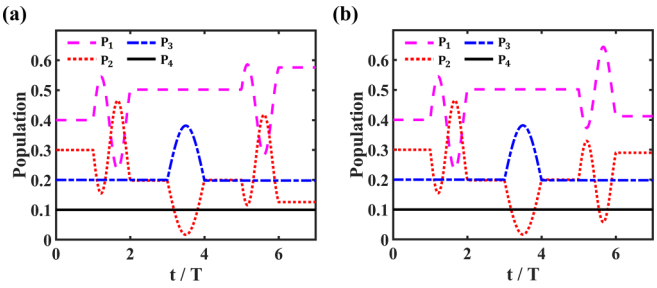

FIG. 6. (a) Population dynamics against braiding $\pi_{12,u}\pi_{23,u}\pi_{12,o}$ with additional Hamiltonian H_g adding to all of the π pulses. (b) Population dynamics against braiding $\pi_{12,o}\pi_{23,u}\pi_{12,o}$ with additional Hamiltonian H_g adding to all of the π pulses. Through detecting the breaking dynamics we can distinguish the braiding with the same linking pattern but different wringing patterns. Pink dashed lines, population of $|\lambda_1\rangle$, P_1; red dotted lines, population of $|\lambda_2\rangle$, P_2; blue dash-dotted lines, population of $|\lambda_3\rangle$, P_3; black solid lines, population of $|\lambda_4\rangle$, P_4.

2. Effect of initial mixed states on quantum braiding

Here we discuss the distinction of braiding of different input states, pure states and mixed states, while the braiding operations are still coherent. The input states now are described by the density operator as

$$\rho_0 = \begin{pmatrix} |c_1|^2 & \eta c_1 c_2^* & \eta c_1 c_3^* & \eta c_1 c_4^* \\ \eta c_2 c_1^* & |c_2|^2 & \eta c_2 c_3^* & \eta c_2 c_4^* \\ \eta c_3 c_1^* & \eta c_3 c_2^* & |c_3|^2 & \eta c_3 c_4^* \\ \eta c_4 c_1^* & \eta c_4 c_2^* & \eta c_4 c_3^* & |c_4|^2 \end{pmatrix}. \tag{A4}$$

The density operator is a pure state when $\eta = 1$ and is mixed state when $0 \leqslant \eta < 1$; c_i, $i = 1, 2, 3, 4$ are probability amplitudes of $|i\rangle$.

In Fig. 5, the population dynamics of the braiding upon eigenstates $|\lambda_{2,3}\rangle$ are shown, where the control parameters are the same as the ones in Fig. 2 and $c_1 = \sqrt{0.4}$, $c_2 = \sqrt{0.3}$, $c_3 = \sqrt{0.2}$, $c_4 = \sqrt{0.1}$. We consider union operations of $\pi_{23,u}$ with $\phi = \pi/2$. The density operator is computed by $\rho(t) = U_c \rho_0 U_c^\dagger$, $U_c = U_H(T_2)U_\pi(T)U_H(T_1)$, $U_\pi(T) = \pi_{23,u}$. The red (population of $|\lambda_2\rangle$, P_{p2}) and blue (population of $|\lambda_3\rangle$, P_{p3}) solid lines in Fig. 5 are the numerical results of pure states with $\eta = 1$ in Eq. (A4). Since the initial state and the braiding are both coherent, the dynamics of the population will be subject to the phase ϕ sinusoidally. The red (blue) dotted lines are the results of $P_{t2}(P_{t3})$ with the situation of $\eta = 0$. Here the input state is classical, of which the population dynamics will not change as one tilts the phase ϕ. A common case of $\eta = 1/2$ is shown by the red (blue) dashed lines in Fig. 5 where the population dynamics of $P_{m2}(P_{m3})$ can be subjected to the phase variation of ϕ but will not be as perfect as the case in $\eta = 1$. Therefore, a quantum braiding needs the input state and the braiding operations to be both coherent.

3. Characterizing the wringing pattern with breaking dynamics

Taking advantage of the full controllability of the proposed system, we can test the braiding topology by breaking the braiding which can be done by adding a global Hamiltonian to the braiding operations.

As in the case of Fig. 4(a), two braidings with the same linking pattern but different wringing patterns cannot be distinguished by the population of the output states, that is function K. However, through applying a specific (but not unique) Hamiltonian

$$H_g = \Omega_0 \begin{pmatrix} 0 & -1 & 0 & 0 \\ -1 & 0 & 0 & 0 \\ 0 & 0 & -1 & 0 \\ 0 & 0 & 0 & -1 \end{pmatrix}, \tag{A5}$$

to all of the π pulses, the results will be different. The numerical results are shown in Figs. 6(a) and 6(b). The evolution operator of Fig. 6(a) is derived as

$$U_{ag} = U_{H_g - H_{12}} U_{H_g - H_{23}} U_{H_g + H_{12}}, \tag{A6}$$

while the evolution operator of Fig. 6(b) is derived as

$$U_{bg} = U_{H_g + H_{12}} U_{H_g - H_{23}} U_{H_g + H_{12}}, \tag{A7}$$

where $U_{H'} = e^{-iH'T}$. The initial states and the control parameters are the same as the ones in Figs. 2(a) and 2(b). The existence of H_g breaks the configurations of U_a and U_b since operators $U_{H_g+H_{12}}(U_{H_g-H_{12}})$ are no longer π pulses. The evolution will be dynamically dependent on $\Omega_0 T$ yet still inside the threefold-degenerate eigensubspace. In Figs. 6(a) and 6(b), one can easily find that the final populations P_i, $i = 1, 2, 3$, are different for U_{ag} and U_{bg}. Consequently, we can describe the topology of braiding by function K and breaking dynamics.

4. Qutrit gates in degenerate eigensubspace

d-ary digits ($d > 2$) encoded in multiquantum states have emerged as an alternative way to qubit for quantum computation and quantum information science. Due to the larger Hilbert space, d-ary digits feature a more powerful ability to do multiple control operations simultaneously and reduce the circuit complexity, simplifying the experimental setup and enhancing the algorithm efficiency [66,67]. Here we investigate the realization of geometric qutrit gates in the threefold-degenerate eigensubspace with Hamiltonian (1), i.e., the Pauli X gate X_3 and the Z gate Z_3 with the form

$$X_3 = \begin{pmatrix} 0 & 0 & 1 \\ 1 & 0 & 0 \\ 0 & 1 & 0 \end{pmatrix}, \quad Z_3 = \begin{pmatrix} 1 & 0 & 0 \\ 0 & e^{i\phi_3} & 0 \\ 0 & 0 & e^{2i\phi_3} \end{pmatrix}. \tag{A8}$$

One can find that the X_3 gate is the cyclic permutation of the probability amplitudes of the quantum state and can be achieved by a pulse sequence of $\pi_{12,o}\pi_{23,o}$. Furthermore, the Z_3 gate can be achieved by the sequences $\pi_{23,u}(\phi_3)\pi_{23,o}(0)\pi_{12,u}(\phi_3)\pi_{12,o}(0)$ where zero or ϕ_3 in $\phi_{kj,o(u)}$ can be determined by the ϕ_{kj} in Eqs. (5) and (6). The operation $\pi_{kj,o(u)}$ can be realized geometrically and thus the X_3, Z_3 gates [36–45]. The present control can be also generalized to the case of d-ary digits with n-fold degenerate eigensubspace. Since the eigenstates are connected to the bare states with Eq. (7), therefore, the proposed gates can be applied to the bare states after a unitary transformation.

[1] C. Nayak, S. H. Simon, A. Stern, M. Freedman, and S. D. Sarma, Non-Abelian anyons and topological quantum computation, Rev. Mod. Phys. **80**, 1083 (2008).

[2] A. Kitaev, Fault-tolerant quantum computation by anyons, Ann. Phys. **303**, 2 (2003).

[3] M. Freedman, M. Larsen, and Z. Wang, A modular functor which is universal for quantum computation, Commun. Math. Phys. **227**, 605 (2002).

[4] S. L. Zhu, L. B. Shao, Z. D. Wang, and L. M. Duan, Probing non-Abelian statistics of Majorana fermions in ultracold atomic superfluid, Phys. Rev. Lett. **106**, 100404 (2011).

[5] G. Moore and N. Read, Nonabelions in the fractional quantum hall effect, Nucl. Phys. B **360**, 362 (1991).

[6] P. Bonderson, A. Kitaev, and K. Shtengel, Detecting non-Abelian statistics in the $\nu = 5/2$ fractional quantum Hall state, Phys. Rev. Lett. **96**, 016803 (2006).

[7] D. L. Deng, S. T. Wang, K. Sun, and L. M. Duan, Proposal for observation non-Abelian statistic of Majorana-Schockley fermions in an optical lattices, Phys. Rev. B **91**, 094513 (2015).

[8] D. A. Ivanov, Non-Abelian statistics of half-quantum vortices in p-wave superconductors, Phys. Rev. Lett. **86**, 268 (2001).

[9] J. Alicea, Y. Oreg, G. Refael, F. V. Oppen, and M. P. A. Fisher, Non-Abelian statistics and topological quantum information processing in 1D wire networks, Nat. Phys. **7**, 412 (2011).

[10] Google Quantum AI and Collaborators, Non-Abelian braiding of graph vertices in a superconducting processor, Nature (London) **618**, 264 (2023).

[11] S. B. Xu, Z. Z. Sun, K. Wang, L. Xiang, Z. T. Zhu, F. H. Shen, Z. X. Song, P. F. Zhang, W. H. Ren, X. Zhang, H. Dong, J. F. Deng, J. C. Chen, Y. Z. Wu, Z. Q. Tan, Y. Gao, F. T. Jin, X. H. Zhu, C. Y. Zhang, N. Wang *et al.*, Digital simulation of non-Abelian anyons with 68 programmable superconducting qubits, Chin. Phys. Lett. **40**, 060301 (2023).

[12] X. L. Zhang, F. Yu, Z. G. Chen, Z. N. Tian, Q. D. Chen, H. B. Sun, and G. C. Ma, Non-Abelian braiding on photonic chips, Nat. Photonics **16**, 390 (2022).

[13] S. Scheel and A. Szameit, A braid for light, Nat. Photonics **16**, 344 (2022).

[14] Z. G. Chen, R. Y. Zhang, C. T. Chan, and G. C. Ma, Classical non-Abelian braiding of acoustic modes, Nat. Phys. **18**, 179 (2022).

[15] Y. T. Chen, R. Y. Zhang, Z. F. Xiong, Z. H. Hang, J. S. Li, J. Q. Shen, and C. T. Chan, Non-Abelian gauge field optics, Nat. Commun. **10**, 3125 (2019).

[16] Q. H. Guo, T. S. Jiang, R. Y. Zhang, L. Zhang, Z. Q. Zhang, B. Yang, S. Zhang, and C. T. Chan, Experimental observation of non-Abelian topological charges and edge states, Nature (London) **594**, 195 (2021).

[17] V. Neef, J. Pinske, F. Klauck, L. Teuber, M. Kremer, M. Ehrhardt, M. Heinrich, S. Scheel, and A. Szameit, Three-dimensional non-Abelian quantum holonomy, Nat. Phys. **19**, 30 (2023).

[18] C. C. Wojcik, X.-Q. Sun, T. Bzdušek, and S. Fan, Homotopy characterization of non-Hermitian Hamiltonians, Phys. Rev. B **101**, 205417 (2020).

[19] Z. Li and R. S. K. Mong, Homotopical classification of non-Hermitian band structures, Phys. Rev. B **103**, 155129 (2021).

[20] Z. Yang, C.-K. Chiu, C. Fang, and J. Hu, Jones Polynomial and knot transitions in Hermitian and non-Hermitian topological semimetals, Phys. Rev. Lett. **124**, 186402 (2020).

[21] H. P. Hu and E. H. Zhang, Knots and non-Hermitian Bloch bands, Phys. Rev. Lett. **126**, 010401 (2021).

[22] H. P. Hu, S. K. Sun, and S. Chen, Knot topology of exceptional point and non-Hermitian no-go theorem, Phys. Rev. Res. **4**, L022064 (2022).

[23] F. N. Ünal, A. Bouhon, and R. J. Slager, Topological Euler class as a dynamical observable in optical lattices, Phys. Rev. Lett. **125**, 053601 (2020).

[24] B. Jiang, A. Bouhon, Z. K. Lin, X. X. Zhou, B. Hou, F. Li, R. J. Slager, and J. H. Jiang, Experimental observation of non-Abelian topological acoustic semimetals and their phase transitions, Nat. Phys. **17**, 1239 (2021).

[25] A. Bouhon, Q. S. Wu, R. J. Slager, H. M. Weng, O. V. Yazyev, and T. Bzdušek, Non-Abelian reciprocal braiding of Weyl points and its manifestation in ZrTex, Nat. Phys. **16**, 1137 (2020).

[26] R. Barnett, G. R. Boyd, and V. Galitski, SU(3) spin-orbit coupling in systems of ultracold atoms, Phys. Rev. Lett. **109**, 235308 (2012).

[27] Y. X. Hu, C. Miniatura, D. Wilkowski, and B. Gremaud, U(3) artificial gauge fields for cold atoms, Phys. Rev. A **90**, 023601 (2014).

[28] Q. X. Lv, Y. X. Du, Z. T. Liang, H. Z. Liu, J. H. Liang, L. Q. Chen, L. M. Zhou, S. C. Zhang, D. W. Zhang, B. Q. Ai, H. Yan, and S. L. Zhu, Measurement of spin Chern numbers in quantum simulated topological insulators, Phys. Rev. Lett. **127**, 136802 (2021).

[29] S. Sugawa, F. S. Carcoba, A. R. Perry, Y. Yue, and I. B. Spielman, Second Chern number of a quantum-simulated non-Abelian Yang monopole, Science **360**, 1429 (2018).

[30] S. Sugawa, F. S. Carcoba, Y. Yue, A. Putra, and I. B. Spielman, Wilson loop and Wilczek-Zee phase from a non-Abelian gauge field, npj Quantum Inf. **7**, 144 (2021).

[31] Y. J. Lin, G. Jimenez, and I. B. Spielman, Spin orbit-coupled Bose-Einstein condensates, Nature (London) **471**, 83 (2011).

[32] F. Leroux, K. Pandey, R. Rebhi, F. Chevy, C. Miniatura, B. Gremaud, and D. Wilkowski, Non-Abelian adiabatic geometric transformations in a cold strontium gas, Nat. Commun. **9**, 3580 (2018).

[33] D. W. Zhang, Y. Q. Zhu, Y. X. Zhao, H. Yan, and S. L. Zhu, Topological quantum matter with cold atoms, Adv. Phys. **67**, 253 (2018).

[34] F. Wilczek and A. Zee, Appearance of gauge structure in simple dynamical systems, Phys. Rev. Lett. **52**, 2111 (1984).

[35] L. M. Duan, J. I. Cirac, and P. Zoller, Geometric manipulation of trapped ions for quantum computation, Science **292**, 1695 (2001).

[36] E. Sjöqvist, D. M. Tong, L. M. Andersson, B. Hessmo, M. Johansson, and K. Singh, Non-adiabatic holonomic quantum computation, New J. Phys. **14**, 103035 (2012).

[37] A. A. Abdumalikov Jr, J. M. Fink, K. Juliusson, M. Pechal, S. Berger, A. Wallraff, and S. Filipp, Experimental realization of non-Abelian non-adiabatic geometric gates, Nature (London) **496**, 482 (2013).

[38] C. Zu, W. B. Wang, L. He, W. G. Zhang, C. Y. Dai, F. Wang, and L. M. Duan, Experimental realization of universal geometric

quantum gates with solid-state spins, Nature (London) **514**, 72 (2014).

[39] K. Toyoda, K. Uchida, A. Noguchi, S. Haze, and S. Urabe, Realization of holonomic single-qubit operations, Phys. Rev. A **87**, 052307 (2013).

[40] S. L. Zhu and Z. D. Wang, Implementation of universal quantum gates based on nonadiabatic geometric phases, Phys. Rev. Lett. **89**, 097902 (2002).

[41] Y. Xu, W. Cai, Y. Ma, X. Mu, L. Hu, T. Chen, H. Wang, Y. P. Song, Z. Y. Xue, Z. Q. Yin, and L. Sun, Single-loop realization of arbitrary non-adiabatic holonomic single-qubit quantum gates in a superconducting circuit, Phys. Rev. Lett. **121**, 110501 (2018).

[42] T. Chen and Z. Y. Xue, Nonadiabatic geometric quantum computation with parametrically tunable coupling, Phys. Rev. Appl. **10**, 054051 (2018).

[43] S. Li and Z. Y. Xue, Dynamically corrected nonadiabatic holonomic quantum gates, Phys. Rev. Appl. **16**, 044005 (2021).

[44] Y. Liang, P. Shen, T. Chen, and Z. Y. Xue, Nonadiabatic holonomic quantum computation and its optimal control, Sci. China Inf. Sci. **66**, 180502 (2023).

[45] Y. X. Du, B. J. Liu, Q. X. Lv, X. D. Zhang, H. Yan, and S. L. Zhu, Degenerate eigensubspace in a triangle-level system and its geometric quantum control, Phys. Rev. A **96**, 012333 (2017).

[46] S. L. Zhu, H. Fu, C. J. Wu, S. C. Zhang, and L. M. Duan, Spin Hall effects for cold atoms in a light-induced gauge potential, Phys. Rev. Lett. **97**, 240401 (2006).

[47] C. C. Adams and T. R. Govindarajan, The knot book: An elementary introduction to the mathematical theory of knots, Phys. Today **48**(4), 89 (1995).

[48] C. N. Yang and M.-L. Ge, *Braid Group, Knot Theory and Statistical Mechanics II* (World Scientific, Singapore, 1994).

[49] R. Freivalds, Knot theory, Jones polynomial and quantum computing, in *Mathematical Foundations of Computer Science 2005* (Springer-Verlag, Berlin, 2005), pp. 15–25.

[50] The avoid-crossing operation can be defined as $\pi_{kj,a} = \pm i(\cos\beta|\lambda_k\rangle\langle\lambda_j|e^{i\phi_{kj}} + \cos\beta|\lambda_j\rangle\langle\lambda_k|e^{-i\phi_{kj}} + \sin\beta|\lambda_k\rangle\langle\lambda_k| + \sin\beta|\lambda_j\rangle\langle\lambda_j|) + |\lambda_l\rangle\langle\lambda_l| + |\lambda_4\rangle\langle\lambda_4|$; β can be either time dependent or time independent.

[51] Note that the initial values of θ, α, and φ are arbitrary; however, the present setting will be the best simplicity after considering the experimental realization.

[52] In this case, the coupling terms in Hamiltonian (1) are given by $\Omega_1 = \Omega_0, \Omega_2 = \Omega_3 = \Omega_4 = 0, \Delta_1 = \Delta_2 = -\Omega_0$.

[53] G. P. Collins, Computing with quantum knots, Sci. Am. **294**, 56 (2006).

[54] M. D. Schroer, M. Kolodrubetz, W. Kindel, M. Sandberg, J. Gao, M. Vissers, D. Pappas, A. Polkovnikov, and K. Lehnert, Measuring a topological transition in an artificial spin-1/2 system, Phys. Rev. Lett. **113**, 050402 (2014).

[55] P. Roushan, C. Neill, Y. Chen, M. Kolodrubetz, C. Quintana, N. Leung, M. Fang, R. Barends, B. Campbell, Z. Chen, B. Chiaro, A. Dunsworth, E. Jeffrey, J. Kelly, A. Megrant, J. Mutus, P. J. J. O'Malley, D. Sank, A. Vainsencher, J. Wenner *et al.*, Observation of topological transitions in interacting quantum circuits, Nature (London) **515**, 241 (2014).

[56] X. S. Tan, D. W. Zhang, W. Zheng, X. P. Yang, S. Q. Song, Z. K. Han, Y. Q. Dong, Z. M. Wang, D. Lan, H. Yan, S. L. Zhu, and Y. Yu, Experimental observation of tensor monopoles with a superconducting qudit, Phys. Rev. Lett. **126**, 017702 (2021).

[57] C. Zheng, J. L. Li, S. Y. Song, and G. L. Long, Direct experimental simulation of the Yang-Baxter equation, J. Opt. Soc. Am. B **30**, 1688 (2013).

[58] F. A. Vind, A. Foerster, I. S. Oliveira, R. S. Sarthour, D. O. Soares-Pinto, A. M. Souza, and I. Roditi, Experimental realization of the Yang-Baxter equation via NMR interferometry, Sci. Rep. **6**, 20789 (2016).

[59] H. Wang, S. J. Wei, C. Zheng, X. Y. Kong, J. W. Wen, X. F. Nie, J. Li, D. W. Lu, and T. Xin, Experimental simulation of the four-dimensional Yang-Baxter equation on a spin quantum simulator, Phys. Rev. A **102**, 012610 (2020).

[60] It should be noted that the writhe ω is not a topological invariant.

[61] M. Saffman and K. Molmer, Scaling the neutral-atom Rydberg gate quantum computer by collective encoding in holmium atoms, Phys. Rev. A **78**, 012336 (2008).

[62] J. Hostetter, J. D. Pritchard, J. E. Lawler, and M. Saffman, Measurement of holmium Rydberg series through magneto-optical trap depletion spectroscopy, Phys. Rev. A **91**, 012507 (2015).

[63] H. Bernien, S. Schwartz, A. Keesling, H. Levine, A. Omran, H. Pichler, S. Choi, A. S. Zibrov, M. Endres, M. Greiner, V. Vuletić, and M. D. Lukin, Probing many-body dynamics on a 51-atom quantum simulator, Nature (London) **551**, 579 (2017).

[64] A. Browaeys and T. Lahaye, Many-body physics with individually controlled Rydberg atoms, Nat. Phys. **16**, 132 (2020).

[65] C. Chen, G. Bornet, M. Bintz, G. Emperauger, L. Leclerc, V. S. Liu, P. Scholl, D. Barredo, J. Hauschild, S. Chatterjee, M. Schuler, A. M. Läuchli, M. P. Zaletel, T. Lahaye, N. Y. Yao, and A. Browaeys, Continuous symmetry breaking in a two-dimensional Rydberg array, Nature (London) **616**, 691 (2023).

[66] A. B. Klimov, R. Guzmán, J. C. Retamal, and C. Saavedra, Qutrit quantum computer with trapped ions, Phys. Rev. A **67**, 062313 (2003).

[67] Y. C. Wang, Z. X. Hu, B. C. Sanders, and S. Kais, Qudits and high-dimensional quantum computing, Front. Phys. **8**, 589504 (2020).